CLM - P 453

UKAEA RESEARCH GROUP

Preprint

NON-SPHERICAL BUBBLE COLLAPSE IN AN IDEAL FLUID

P J FIELDING
M K BEVIR

CULHAM LABORATORY
Abingdon Oxfordshire

1976

CLM-P 453

NON-SPHERICAL BUBBLE COLLAPSE IN AN IDEAL FLUID

by

P.J. Fielding and M.K. Bevir

ABSTRACT

The collapse of initially spherical, vapour- or gas-filled cavities within a liquid, adjacent to a solid wall, or in other axially symmetric situations, is often characterised by the formation of imploding high-speed liquid jets, which are of interest in the study of cavitation damage, for example. A fast, new, numerical method is described here for the solution of cavity collapse and other bubble dynamics problems possessing axisymmetry. Viscosity and compressibility are neglected in the liquid flow, which is assumed irrotational, and the effects of heat and mass transfer across the bubble wall are neglected also. Several examples are presented, illustrating cavity collapse near a solid wall, and under gravity, with and without surface tension on the bubble wall.

(Paper presented at Institute of Physics 3rd National Computational Physics Conference, Glasgow, 27-29 August 1975.)

UKAEA Research Group
Culham Laboratory
Abingdon Oxon
OX14 3DB

January 1976

I. INTRODUCTION

Interest in the behaviour of gas-filled bubbles and other cavities within liquids is common to several areas of study in fluid dynamics, including boiling heat transfer, cavitation, and under-sea explosions. It has long been known from experimental work,[1] and more recently from numerical calculation,[2] that under many conditions of interest, initially spherical cavities acted upon by a pressure excess will form high-speed jets of liquid as they collapse. The formation of these jets requires some departure from spherical symmetry in the ambient conditions, such as a density gradient in the liquid, proximity of the cavity to a solid surface, or gravity. The impact of liquid jets is thought to be the cause of damage to solid surfaces exposed to a cavitating liquid,[3] and to be responsible for intense sound production in a liquid boiling near a heated surface. Jet impact may also increase the heat transfer between liquids in fuel-coolant interactions,[4] by enlarging the area of contact.

The development of a numerical method of sufficient accuracy and speed to allow systematic investigation of jet formation, has been the main aim of the present work, and forms the completion of some initial studies, described elsewhere.[5] The formulation of the problem is sufficiently general to allow also the investigation of bubble growth at a heated interface, for example, provided the rate of introduction of vapour into the bubble is specified. At present heat conduction across the interface is not included although this could perhaps be introduced using a thin thermal boundary-layer approximation.[6]

II. EQUATIONS OF FLUID AND CAVITY

The problem we solve then, is the time-dependent motion of a cavity surface within an incompressible liquid in an axisymmetric situation. The pressure far from the cavity $p_\infty(t)$, and the pressure within the cavity $p(t)$, are prescribed. Alternatively, the internal pressure may be calculated using the cavity volume and some gas law. The liquid flow is in all cases irrotational, and viscosity is neglected, so that a fluid potential φ

may be defined, satisfying

$$\nabla^2 \varphi = 0 \qquad (1)$$

and such that the liquid velocity $\underset{\sim}{v} = \nabla\varphi$. The boundary condition infinitely far from the cavity is $\underset{\sim}{v} = 0$, so we may take $\varphi = 0$ at infinity. If a solid wall is present then at each point $\hat{n}.\nabla\varphi = 0$ where $\hat{n}$ is normal to the wall. The boundary condition at the cavity surface is obtained, for a liquid of constant density ρ , acted upon by gravity g , from Bernouilli's equation in unsteady flow,[7] applied to the interface:

$$\frac{D\varphi}{Dt} = \frac{p_\infty - p}{\rho} - g(x_o - x) + \frac{\sigma}{\rho}\left(\frac{1}{R_1} + \frac{1}{R_2}\right) + \frac{1}{2} v^2 \qquad (2)$$

where the Lagrangian time-derivative of φ at points on the interface is given by

$$\frac{D\varphi}{Dt} = \frac{\partial\varphi}{\partial t} + v^2 \ ,$$

v being the fluid velocity, and σ is the constant of surface tension, R_1 and R_2 being principal radii of curvature. The vertical height, x , of each point is measured along the symmetry axis from an arbitrary reference level for p_∞ , at x_o .

The kinematic conditions

$$\frac{dr}{dt} = \hat{r}.\nabla\varphi \qquad \text{and} \qquad \frac{dx}{dt} = \hat{x}.\nabla\varphi \qquad (3)$$

describe the motion of the interface in terms of the cylindrical coordinates (r,x) of each of its points.

Equations 1 → 3 can be written in non-dimensional form by expressing pressures, density and length in terms of scaling values P_o , ρ_o , and L_o respectively. The unit of velocity is then $\sqrt{P_o/\rho_o}$, of time $L_o\sqrt{\rho_o/P_o}$, of gravity $\left(\frac{P_o}{L_o\rho_o}\right)$ and of surface tension, (P_oL_o) .

III. METHOD OF SOLUTION

(a) The Boundary-value problem

Given the position of the interface at any instant and the corresponding values of potential there, the Laplacian problem may be solved to give the velocity at each boundary point. Given $p(t)$, the boundary values may be advanced in time using (2) and the interface moved to its new position an instant later using (3).

Although the boundary-value problem is mathematically simple, the changing shape of the interface makes it impossible to obtain solutions analytically except where there is a high degree of symmetry, so numerical methods must in general be used. Plesset and Chapman obtained numerical solutions of (1) - (3) for cavity collapse adjacent to a wall by setting up a number of meshes in cylindrical coordinates, the cell-size increasing with distance from the cavity. They then solved the boundary-value problem for φ, at each timestep by finite difference methods involving an iterative matching procedure between the numerical solution and an asymptotic form supposed valid beyond the outer boundary of the mesh, and satisfying the boundary condition at infinity. An Eulerian time-difference was employed to advance the solution variables. The interface was represented by a sequence of nodes, and the boundary condition on φ was applied to the computation mesh by interpolation. Although no calculation times are quoted, this is likely to be a slow method for obtaining the velocity of the interface.

(b) Green's Function Method

In order to solve the potential problem more succinctly we have instead developed a Green's function method which allows the interface velocity to be computed entirely in terms of integrals and functions defined on the interface. Large two-dimensional finite difference meshes are thus avoided, being replaced by square matrices of modest dimensions, and in addition to being fast, the method has the added advantage of providing simple and reliable estimates of the local solution error.

Making use of rotational symmetry, we represent the cavity by its cross-section L, as in figure 1. Denoting distance along L by s, it may be shown that provided L has continuously-turning tangent, and the boundary potential φ has a continuous, bounded tangential derivative, then a bounded, continuous function $q(s)$ exists, satisfying the following integral equation:

$$\int_0^S G(\underset{\sim}{r}(s)/\underset{\sim}{r}(s'))\ q(s')ds' = \varphi(s)\ ,\ 0 \leqslant s \leqslant S \qquad (4)$$

where $$G(\underset{\sim}{r}/\underset{\sim}{r}') = \frac{r'K(k)}{\sqrt{\{(x - x')^2 + (r + r')^2\}}}$$

and $$k^2 = \frac{4rr'}{\{(x - x')^2 + (r + r')^2\}}\ ,$$

$K(k)$ being the complete elliptic integral of first kind. $G(\underset{\sim}{r}/\underset{\sim}{r}')$ is the Green's function which vanishes at infinity, for the Laplacian in axisymmetric geometry, so the harmonic function

$$\varphi(\underset{\sim}{r}) = \int_0^S G(\underset{\sim}{r}/\underset{\sim}{r}(s'))\ \underset{\sim}{q}(s')\ ds' \qquad (5)$$

defined in the region occupied by fluid, is the solution of (1) which satisfies the given boundary conditions. Note that $q(s)$ may be interpreted physically as a distribution of fluid source density over the interface. Differentiation of (5) gives the fluid velocity anywhere in the liquid, unless the point lies on the interface. In this case, by differentiating and then taking the limit in (5) as $\underset{\sim}{r}$ approaches a given boundary point from within the liquid, correct account is taken of the normal discontinuity of grad φ at the interface. Thus, by solving equation (4) for $q(s)$, the values of grad φ at the boundary may be obtained. However, it is important to note that the kernel of this Fredholm equation is singular ($G(\underset{\sim}{r}/\underset{\sim}{r}') \to \frac{1}{2}\ \ell n\ |\frac{8r(s)}{s' - s}|$, as $s' \to s$) unless the field-point $\underset{\sim}{r}(s)$ lies on the symmetry axis. Similarly, the integrand in the limit expression for the velocity obtained from (5) is singular at $s' = s$. By subtracting off the singular part in the integrand

of (4) and evaluating its contribution analytically, the problem of dealing numerically with singularities is avoided. A similar treatment is applied to the evaluation of grad φ at the interface. The problem is discretised for numerical treatment by describing the curve of cross-section L by means of a suitably-chosen distribution of nodes $\{x_m , r_m\}_{m=1}^{M+1}$ along it, and applying equation (4) at each node, the contour shape between the nodes being defined by cubic splines in the parametric variable, s . Since it is generally desirable to work to second-order accuracy in the inter-nodal distances Δs_m , it is assumed that q(s) is a piecewise-linear function of s , changing gradient at the nodes. Then we obtain a matrix equation

$$\sum_{m=1}^{M+1} A_{nm}\, q_m = \varphi_n \ , \quad n = 1 \ , \ \ldots \ , \ M+1 \qquad (6)$$

for the nodal values of source-density, q_m . Provided the matrix elements are evaluated with sufficient accuracy, the matrix A is non-singular. Similar matrix-product expressions are obtained for the nodal velocity components. Observe that A depends only on the geometry of the interface and other boundaries. The presence of a wall is dealt with by the method of images, the general approach being the same, except that singularities do not arise from the image sources.† The detailed expressions used, and techniques involved have been described elsewhere,(8) so it will be sufficient here to note that the resulting velocity solutions are obtained with second-order accuracy in the local segment length Δs_m , there being two principal contributions to the local error, proportional to $\delta_K^2 = (K_m \Delta s_m)^2$ and to $\delta_q^2 = \left\{ \{\partial^2 q/\partial s^2\} \Big/ < q > \right\} \Delta s_m^{\,2}$, where K_m is the local curvature, and $< q >$ is the root-mean-square value of q . The first of these arises in approximating segment-lengths by straight line distances, and the second from the assumption that q(s) is a piecewise linear function. Information about

---

†When the cavity touches a wall this is not strictly true if a point of contact exists away from the axis of symmetry. But in such a situation, mirror symmetry can be used to eliminate the problem of singularity.

these two quantities can, it is clear, be used to optimise the distribution of nodes. Typically, accuracy better than 0.1% is ensured with $\delta_K , \delta_q \lesssim 0.1$.

IV. NUMERICAL AND PROGRAMMING TECHNIQUES

A computer program using the methods outlined above for solving the potential problem has been written to solve the initial-value problem for the interface. The conventions of the OLYMPUS[9] system were employed, the structure of the code being based upon the ARGOS contour-dynamics[10] program developed at Culham. Two methods of time-integration have been examined and may be used as alternatives in the code: the first-order, Eulerian, and the leap-frog, second-order accurate schemes, both being explicit methods.

Thus, for each of the nodes $m = 1 , \ldots M + 1$,

$$x_m(t_{n+1}) = x_m(t_n + \Delta t_n) = x_m(t_n) + f_1(x_m(t_{n-1}) - x_m(t_n)) + f_2 \, v_{xm}(t_n) \qquad (7)$$

with similar equations for the variables r and φ ,

where

$f_1 = 0$ for Eulerian

$= (\Delta t_n / \Delta t_{n-1})^2$ for Leap-frog

and

$f_2 = \Delta t_n$, for Eulerian

$= \Delta t_n (\Delta t_n + \Delta t_{n-1}) / \Delta t_{n-1}$, for Leap-frog.

In order to ensure linear stability of these equations, at each step Δt_n must be chosen to satisfy a condition of the form

$$\omega_{max} \, \Delta t_n < \alpha \qquad (8)$$

where α is a constant of order unity. ω_{max} corresponds to the highest wave-frequency or instability growth-rate for perturbations of the interface. In order of magnitude, ω_{max} is estimated using the plane-wave dispersion

formula $\omega^2 = -ak + \frac{\sigma}{\rho} k^3$, where a is the normal acceleration of the interface, positive when directed towards the liquid. The highest wave-number that may be represented at the m^{th} node is $k_{max} \sim 2\pi/(\Delta s_m + \Delta s_{m-1})$, so $\omega_{max}^2 = \max_{m \in (1, M+1)} \left| -a_m k_{max} + \frac{\sigma}{\rho} k_{max}^3 \right|$ where a_m is the normal acceleration at the m^{th} node on the interface. This neglects the effects of curvature, but has been found quite satisfactory. By experimenting with small amplitude oscillations of a gas-bubble with surface tension on the interface, the value $\alpha = 0.6$ was found to give a 'safe' margin of stability, and this has proved generally satisfactory. When the cavity contains non-condensible gas, there is an additional frequency to be considered, characteristic of the compressional oscillation. But this is neglected since it is always much lower than the maximum surface-wave frequency, for cases of interest. It will be noted that the difference schemes (7) are non-dissipative, in the sense of Kreiss.[11] This is of no consequence for small amplitude motions, but gives rise to numerical difficulties in cavity collapse calculations, which manifest themselves in the form of growing perturbations of the interface, strongly localised in the region of high acceleration where a jet forms, with a local wavelength $\sim \Delta s$. Once they have reached large amplitude, these perturbations give rise to extremely large oscillatory accelerations, which effectively stop the calculation by reducing the timestep by orders of magnitude. The growth of these perturbations can be traced to the curvature-dependent terms which were neglected in estimating the wave-frequency. It is well known that a collapsing spherical cavity is unstable to surface perturbations, the amplitude of perturbation growing asymptotically like $R^{-\frac{1}{4}}$, where R is the unperturbed cavity radius.[12]

Plesset and Mitchell[13] have solved numerically for the linear perturbation amplitudes of spherical, collapsing cavities with and without surface tension and showed that the amplitude growth cannot be limited by surface tension. It is clear that perturbations of the geometry are inevitable in the numerical

solutions due to errors of second-order in the segment-lengths which accompany the evaluation of the interface velocity. Since the growth of such perturbations will be non-exponential, in the case of spherical and - presumably - also for non-spherical collapse, we expect the mild damping of short wavelengths will cause them to be stabilised. The numerical scheme must therefore be modified to make it dissipative (in the sense of Kreiss). This is easily arranged by adding to each of the difference equations (7) a diffusive term, so that the "smoothed" variables, $\bar{x}$, for example, are given in terms of the unsmoothed, x, by relations of the form $\bar{x}_m(t + \Delta t) = x_m(t + \Delta t) + \alpha_m \Delta t \frac{\partial^2 x(t)}{\partial s^2}$, for some α_m. For this modification to be consistent with the desired level of solution accuracy, α_m must be of second order in Δs_m when the flow is perturbation-free. In the presence of a perturbing velocity of magnitude δv_m in the Laplace solver, and characteristic wave number Δs_m^{-1}, the saturation amplitude ϵ, of the perturbation in x is estimated by equating the error per timestep in x, $\delta v_m \Delta t$, and the last term in the diffusion equation. This gives

$$\delta v_m \Delta t \sim \alpha_m \epsilon \Delta t \Big/ \Delta s_m^2 .$$

Since it is desirable that ϵ should saturate at some small fraction of $K_m \Delta s_m^2$ to avoid significant deviations in the local curvature K_m, we see that

$$\alpha_m \sim \delta v_m / |K_m|$$

where the constant of proportionality should be small compared with unity.

Recalling the form of the local velocity-error estimate, we are thus naturally led to the form

$$\alpha_m = \left\{ c_1 \frac{\left|\frac{\partial^2 q}{\partial s^2}\right|}{< q >} \cdot \left|\frac{1}{K_m}\right| + c_2 |K_m| \right\} |v_m| \Delta s_m^2$$

where c_1 and c_2 are small constants. In order to avoid difficulties when $|K_m|$ is small, the factor $|K_m|^{-1}$ is replaced by S, the arc length of L, and in order to make α_m more sensitive to pointwise fluctuations in K, the second term is empirically modified to give the final form used:

$$\alpha_m = \left\{ \frac{c_1 \left|\frac{\partial^2 q}{\partial s^2}\right|_m}{< q >} + c_2 \left|\frac{\partial^2 K}{\partial s^2}\right|_m S \right\} |v_m| S \quad (\Delta s_m + \Delta s_{m-1})^2 . \qquad (9)$$

Typically, $c_1 \approx 0.005$, $c_2 \sim c_1/10$ when surface tension is small, larger values being used when the surface tension term is comparable in magnitude to the driving-pressure term. The addition of these terms in the manner described can give rise to numerical instability when large amounts of diffusion appear, the resulting perturbations then giving rise to even larger values of diffusion coefficient. An additional constraint on the timestep must then be imposed, of the form

$$\alpha_m \Delta t / \Delta s_m^2 < \frac{1}{2} .$$

Since it is undesirable that the rate at which the calculation proceeds should be controlled by the numerical damping, it was decided to apply the 'smoothing' as a separate stage of each timestep. The unsmoothed values at t_{n+1} obtained from (7), are then used as initial values for equations of the form

$$\frac{\partial x}{\partial t} = \alpha(s) \frac{\partial^2 x}{\partial s^2} \quad , \qquad (10)$$

where s_m is the parametric coordinate of the m^{th} node at time t_n, the value of α_m being determined from values at this time. By choosing a subsidiary timestep $\Delta t' = \Delta t/K$, where K is an integer, such that stability in (10) is ensured, the smoothed variables are obtained in K explicit steps of (10). This allows Δt to be determined solely by the hydrodynamics.

V. GROWTH OF NON-UNIFORMITIES - JET FORMATION

It is common for the distortion of cavity-shape, as a result of jet formation say, to result in an initially uniform node-distribution becoming highly non-uniform. In some cases, this is a desirable feature, since it can concentrate nodes in regions of rapid variation. This is by no means universally true, however; and over-concentration of nodes around a jet has the effect of reducing the timestep excessively. In order to deal with this difficulty and in order also to maintain solution accuracy where the node distribution is too sparse, the contour is periodically "adjusted", by applying five criteria at each node, in a semi-iterative manner. These will cause the m^{th} node to be removed if

(1) the tangent to the interface turns through a total angle less than some given minimum between the $(m - 1)^{th}$ and $(m + 1)^{th}$ nodes, and

(2) the source-density second order variation, defined by

$$\left|\frac{\partial^2 q}{\partial s^2}\right| (\Delta s_m + \Delta s_{m-1})^2 \Big/ < q > \text{, is less than some given minimum}$$

or, if this first case does not arise, the m^{th} node may still be removed if the stability restriction (8) gives rise to a timestep less than some given minimum, due to the smallness of $(\Delta s_m + \Delta s_{m-1})$. This results in some sacrifice of accuracy in favour of speed. Equally, a node will be added in the centre of the m^{th} segment if either

(1) the tangent turns through more than a given maximum angle between the m^{th} and $(m + 1)^{th}$ nodes or,

(2) the source-density second order variation, given by

$$\left\{ \left|\frac{\partial^2 q}{\partial s^2}\right|_m + \left|\frac{\partial^2 q}{\partial s^2}\right|_{m+1} \right\} \Delta s_m^2 \Big/ < q >$$

is larger than a given maximum.

The new node then becomes the "$(m + 1)^{th}$" , more nodes being added as required.

Finally, in order to avoid wide variations in the sizes of neighbouring

segments, the m^{th} node will be relocated halfway between the $(m-1)^{th}$ and $(m+1)^{th}$ nodes if the segment length-ratio deviates from unity by more than a given fixed amount.

VI. LEAP-FROG AND EULERIAN SCHEMES COMPARED

Wherever a new node is introduced, or an existing one is relocated, the necessary coordinates and the associated value of potential are obtained from the parametric spline interpolants for the coordinates x, r, and for φ. When using the Eulerian time-difference scheme, adjustment is easily performed at any point in time, as a single operation. However the leap-frog scheme uses information from two time levels, so that it is necessary to ensure that after adjustment both have the same node distribution. This is most conveniently done by "matching" the two time levels, that is by taking the time-centred average, at $(t_{n-1} + t_n)/2$, and adjusting the node distribution on the average interface. Since periodic "matching" is necessary to quench the so-called leap-frog instability[14] which can arise in some problems, this procedure fits naturally into the sequence of operations, although it has been found generally true that the interface must be adjusted much more frequently than it requires to be "matched" to avoid leap-frog instability. Indeed for the problems which have been studied, no evidence of this instability has been found. After adjustments have been made the calculation is restarted by first regenerating the solution at t_{n-1} and then at t_n, by means of the usual "resetting" procedure[14] used in applications of the leap-frog scheme to incompressible hydrodynamics.

It is clear that the Eulerian scheme is simpler to implement. It is also faster, since resetting the leap-frog calculation is equivalent to at least two time-steps.

In comparing results obtained using the two schemes, a useful diagnostic is the total energy integral for the system, given for zero gravity and surface tension, for example, by

$$E = \frac{pV}{\gamma - 1} + p_o V + \frac{1}{2}\rho \int_o^S \varphi \frac{\partial \varphi}{\partial n} ds \ ,$$

where V is the cavity volume, γ is the adiabatic gas constant, and $\frac{\partial \varphi}{\partial n}$ is the inward normal component of fluid velocity at the cavity surface. It is found that for some problems the Eulerian scheme is inadequate if accurate energy conservation is required, although this is not always the case. Generally, however, it is to be expected that accuracy will be significantly higher when the leap-frog scheme is employed.

VII. EXAMPLES OF CAVITY COLLAPSE

Empty Cavities

In the first case we consider, a cavity with zero internal pressure, initially spherical of radius 0.75 and at rest, collapses under unit driving pressure at infinity, the motion becoming aspherical due to gravity, acting in the negative X-direction with strength 0.5. The surface tension coefficient is 0.002. Figure 2 shows a succession of cavity shapes as the collapse proceeds and in figure 3, the jet velocity is shown as a function of time. Since accuracy in the evaluation of velocities rapidly deteriorates when the distance separating the jet tip and the top of the cavity is comparable with the largest neighbouring segment-length, the calculation is effectively stopped as soon as this situation is reached, the final cavity shape together with the time of impact being determined by extrapolation with constant velocity. The dimensionless parameters happen to correspond to a cavity of radius 3.27 cm, collapsing under a driving pressure of 0.009 atm., in water under normal gravity, the units of velocity and time being then 0.93 metres/sec, and 0.047 secs respectively. The impulsive pressure generated by the water-hammer effect of the jet as it strikes the liquid at the upper surface of the cavity may be estimated to be $\frac{1}{2}\rho c v$ where ρ, c are the density and sound speed for water and v is the velocity of impact. Motion of the upper surface being in this case negligible, v is given for the jet velocity, so that an impulsive pressure of the order of 45 atmospheres will be generated.

More violent accelerations and higher jet velocities arise when a vapour

cavity collapses near a wall under the same driving pressure, and as a typical example, solutions have been obtained for one of the problems discussed by Plesset and Chapman[2], in which an empty cavity, initially spherical, of unit radius, collapses against a solid wall under unit driving pressure. Comparison of two solutions, obtained using the Eulerian and leap-frog schemes indicates that energy conservation is maintained at about the same level - around 1% - in both calculations, and that while the jet velocity predicted is the same in both cases, the total collapse time is longer by about 5% using the Eulerian scheme. A further comparison between the figures for jet velocity as a function of time and those quoted in[2] shows reasonable agreement as seen from figure 4. In figure 5, the cavity shape is shown at successive stages of the leap-frog calculation. Oscillations are seen close to the time of collapse, especially in the leap-frog solution, which are difficult to eliminate without applying excessive numerical damping. They appear due to increasing inaccuracy in the velocities towards the end of the collapse, associated with a need for more nodes than is acceptable for rapid completion of the calculation. The difficulty is particularly severe in this case due to the highly involuted final form of the cavity. Consequently, in figure 5, the final extrapolation for the cavity shape at the time of impact has been suppressed, due to the low accuracy of this procedure here.

Nonetheless, by averaging across the fluctuations, it is possible to obtain a satisfactory estimate of final jet velocity, both calculations yielding 13. ± 0.5. As noted in (2), if the initial cavity radius is 1 cm, and the driving pressure is 1 atmosphere, this corresponds to a jet velocity of 130 m/sec, which gives rise to a water-hammer pressure ρcv, of 2,000 atmospheres.

VIII. EFFECT OF NON-CONDENSIBLE GAS

The final example illustrates the effect of non-condensible gas within a collapsing cavity. The investigation of cavity motion is complicated in such cases by the possibility of Rayleigh-Taylor instability during deceleration at the interface, leading to its break-up. When gas obeying an adiabatic law with $\gamma = 5/3$ is included in the cavity collapse adjacent to the wall, considered above, such instability occurs for example, with an initial gas pressure 0.1, the interface becoming unstable soon after the jet forms. If the initial gas pressure is set at a sufficiently low value, however, jet formation will occur without deceleration, and in figure 6 is shown the motion of a unit-radius cavity placed with its centre 1.5 units distant from a solid wall and containing adiabatic gas ($\gamma = 5/3$) at initial pressure 0.005. Surface tension is zero. The final cavity shape has been omitted, since the extrapolation which produces it is inaccurate. Figure 7 gives the variation with time of the gas pressure. At the point of jet impact, this pressure reaches 72 units; however, for most of the time it is less than the external driving pressure, and is unable to decelerate the jet, which reaches a final velocity of 16.5 ± 0.5. This cavity, with a higher unitial gas pressure 0.05, formed a jet which reached a velocity of 10 before starting to decelerate and to become unstable. (At still higher values of initial gas pressure, jets did not form during the first compression of the cavity, though there was some evidence that they may do so in the later stages after the cavity rebounds).

We surmise, in this and other cases where a jet becomes unstable, that its break-up into small droplets of liquid may occur, leading to a significant weakening of water-hammer effects. If so, then even at initial pressures of the order of a few percent of the external driving pressure, non-condensible gas may be capable of suppressing the effects of water-hammering by jets.

Conclusion

The essential numerical features of a computational code describing the collapse of cavities in a liquid have been outlined. The initial shape of the

cavity is prescribed and the fluid motion, assumed incompressible, is caused by a distant pressure field or gravity. The effects of a nearby wall, of surface tension or gas within the bubble are included, but the effects of viscosity and heat conduction in the liquid are not.

A number of examples of cavity collapse and jet formation are presented to illustrate the operation of the code. Empty cavities driven by gravity or collapsing under a pressure field near a wall certainly form jets. However it appears that small quantities of non-condensible gas in the cavity which might be expected to retard jet formation by a simple cushioning effect, also tend to make the jets unstable. It may be that there are lower limits for the initial quantity of non-condensible gas necessary to prevent jet formation, and these may be found by further computation.

Acknowledgment

The authors wish to thank M.H. Hughes and K.W. Morton for helpful discussions, and also to thank M.H. Hughes for the use of his ARGOS subprograms. This work was supported in part by A.E.R.E. Harwell, project no. 4.52.02.

References

1. Benjamin, T.B. and Ellis, A.T., Phil.Trans. Roy. Soc. A260, 221 (1966).

2. Plesset, M.S. and Chapman, R.B., J. Fluid Mech. 47, 283 (1971).

3. Eisenberg, P., Hydronautics, Inc., Laurel, Maryland, Tech. Rep. no. 233-1 (1963).

4. Buchanan, D.J., J. Phys. D: Appl. Phys. 7, 1441 (1974).

5. Bevir, M.K. and Fielding, P.F., paper presented at the Conference on Moving Boundary Problems in Heat Flow and Diffusion, Oxford (1974).

6. Florschuetz, L.W. and Chao, B.T., Trans. ASMEJ Heat Trans. C87, 209 (1965).

7. Landau, L.D. and Lifschitz, E.M., Fluid Mechanics, p.21, Pergamon Press, Oxford (1959).

8. Fielding,P.J. and Bevir, M.K., Culham Laboratory Report CLM-R 146 (1975).

9. Christiansen, J.P. and Roberts, K.V., Computer Physics Communications 7, 245, (1974).

10. Hughes, M.H. and Roberts, K.V., private communication.

11. Richtmeyer, R.D. and Morton, K.W., Difference Methods for Initial Value Problems, Interscience Publishers, New York (1967).

12. Birkhoff, G., Q. Appl. Math. 12, 306 (1954).

13. Plesset, M.S. and Mitchell, T.P., Q. Appl. Math. 13, 419 (1956).

14. Berk, H.L. and Roberts, K.V., Methods in Computational Physics, vol. 9, p.111, Academic Press, 1970.

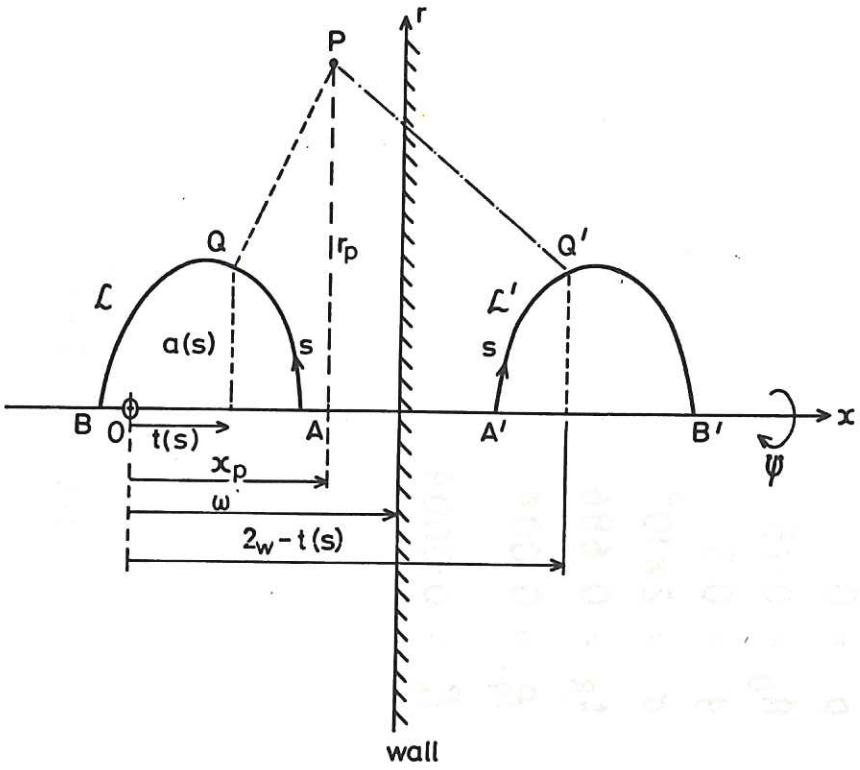

Fig.1 Axisymmetric boundary geometry. $0x$ is the axis of rotational symmetry. If a solid wall is present, at $x = \omega$, there is reflection symmetry about this plane, A′ being the image of A, etc.

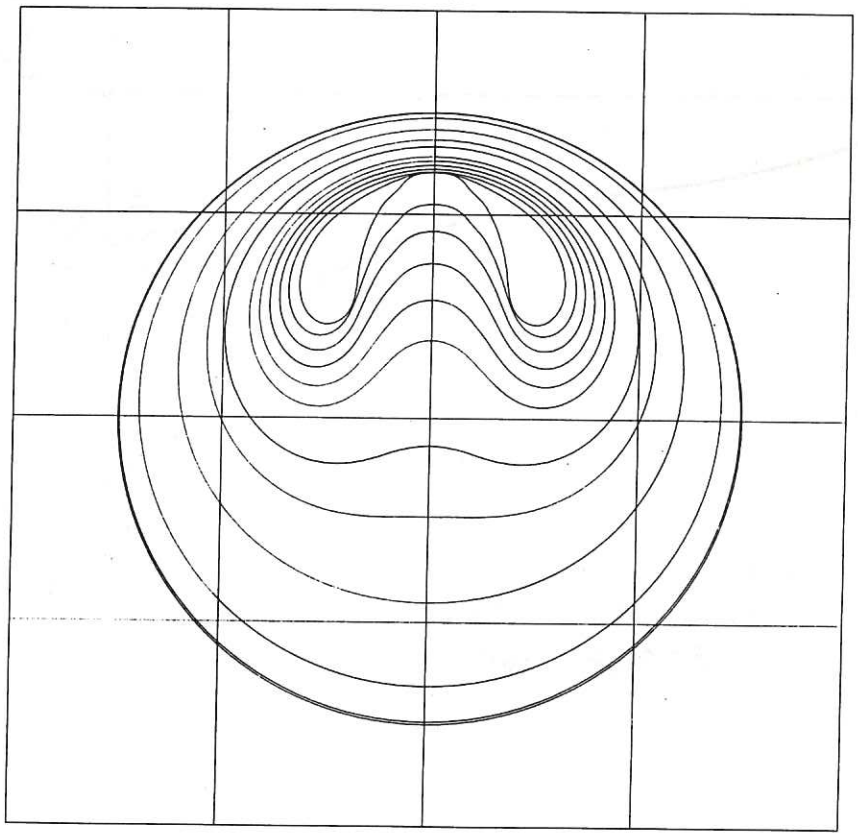

Fig.2 Cavity collapse in the presence of gravity. An empty cavity of initial radius 0.75 collapses under the action of unit driving pressure at infinity. Gravity acts in the negative x - direction (down) with strength 0.5. Surface tension is 0.002.

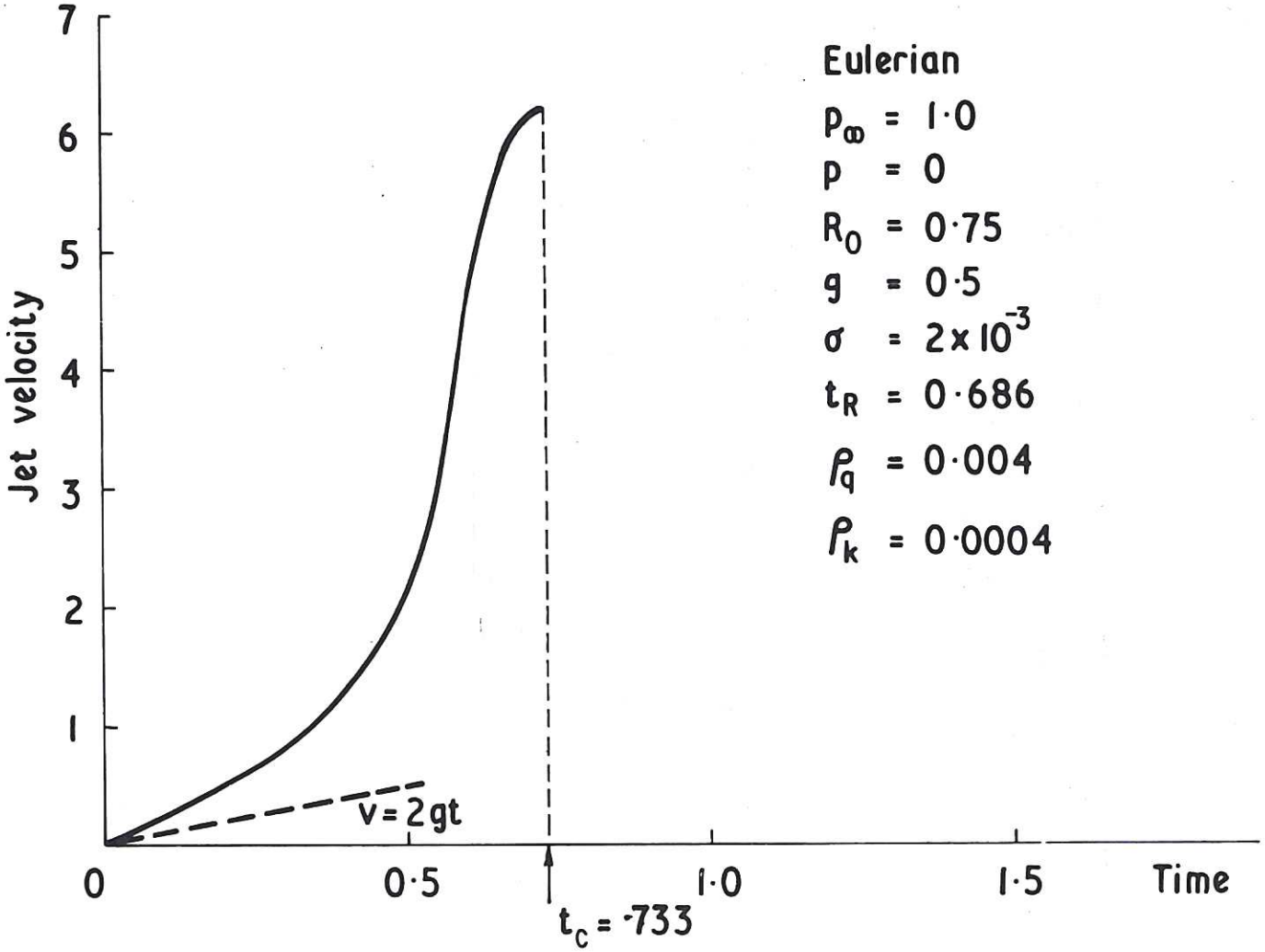

Fig.3 Jet velocity vs time for the gravity collapse depicted in Fig.2. ρ_q, ρ_K are the numerical damping coefficients associated with the source function q and curvature, K, respectively.

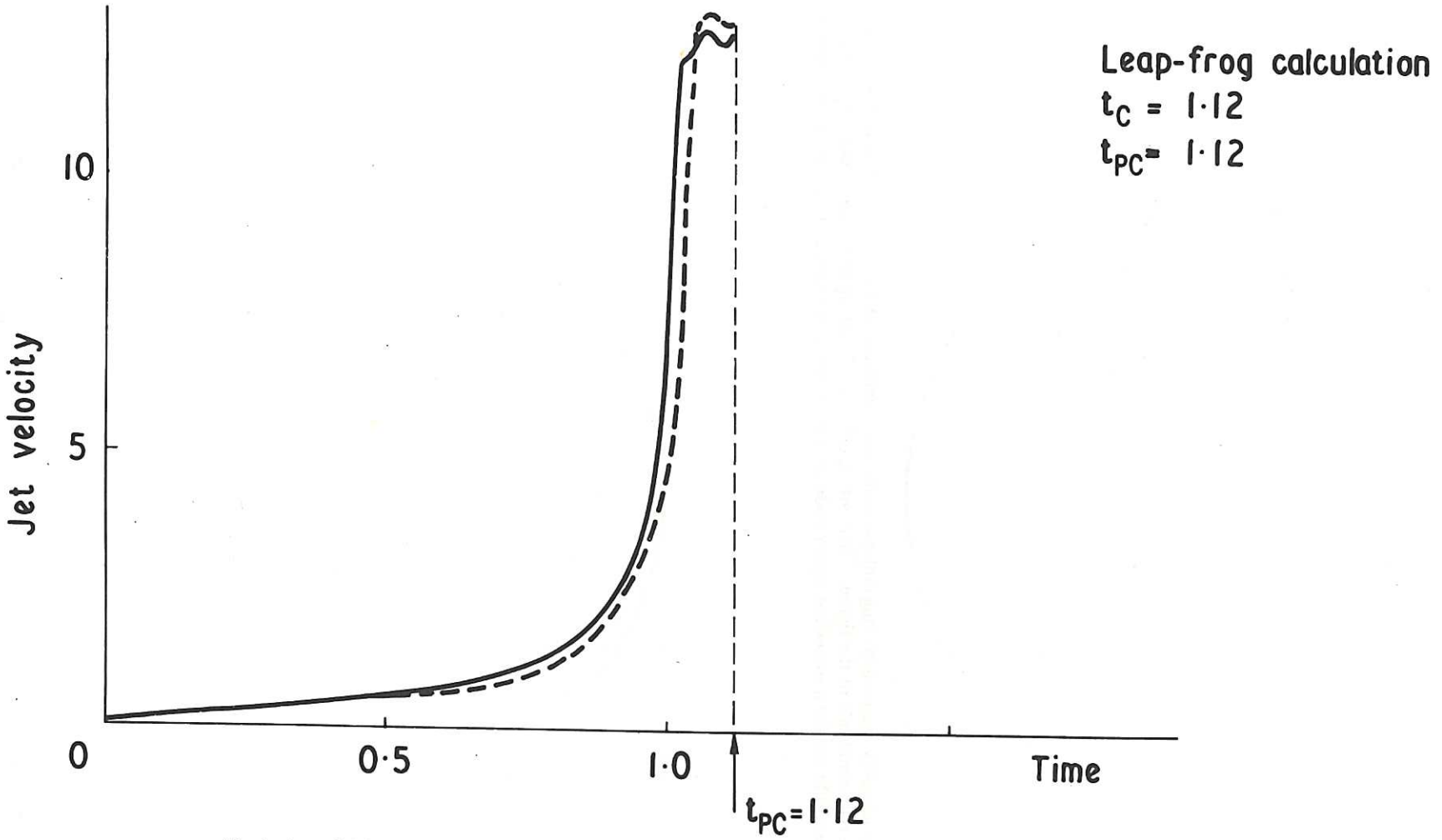

Fig.4 Jet velocity vs time for an empty cavity, initially of unit radius collapsing against a solid wall under unit driving pressure, with surface tension 7.6×10^{-5}. The Leap-frog scheme (solid curve) is compared with the results of Plesset and Chapman[2] (dashed curve) for the same calculation with zero surface tension.

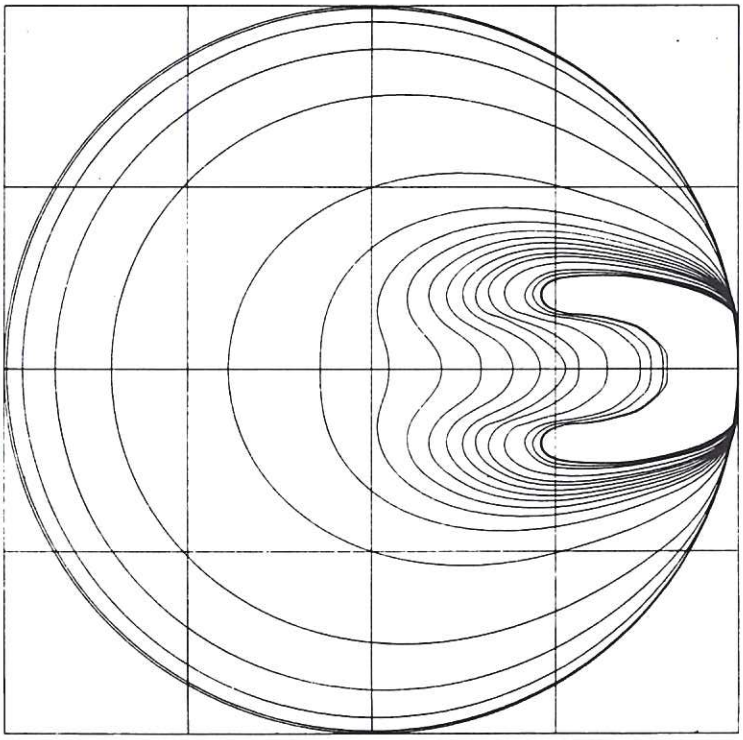

Fig.5 Succession of cavity shapes depicting collapse under the conditions of Fig.4. The wall is in contact with the cavity on the right-hand side of the figure. There are ripples near the jet tip in the later stages of collapse. Removal of these would require a somewhat higher node density on the outer flanks of the cavity than was in fact permitted.

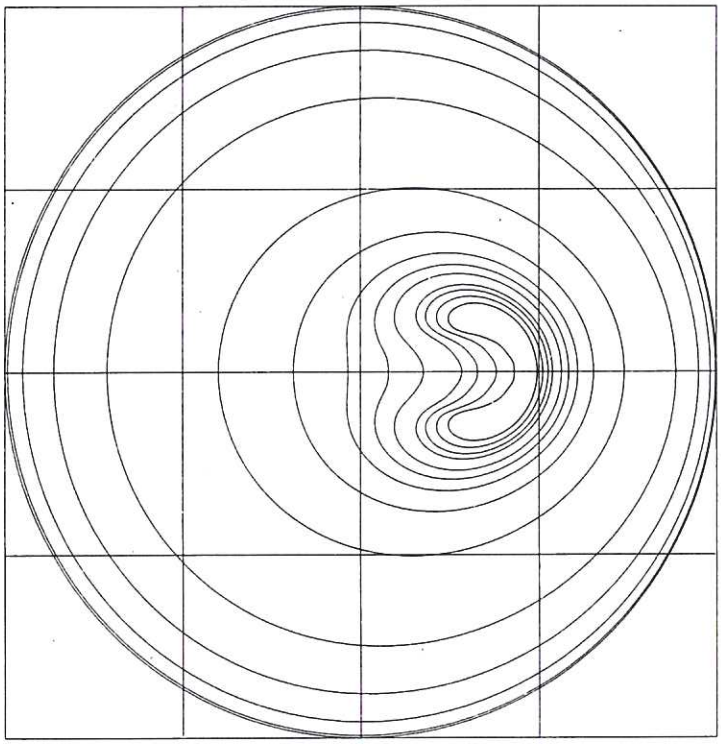

Fig.6 Collapse of a cavity containing gas which obeys the adiabatic law with $\gamma = {}^{5}/_{3}$, adjacent to a solid wall. The cavity is initially spherical, of unit radius and is located 1.5 units distant from the wall, which lies on the right, out of view in the figure. Initial gas pressure is 0.005, the interface is surface-tension-free, and collapse is driven by unit pressure at infinity.

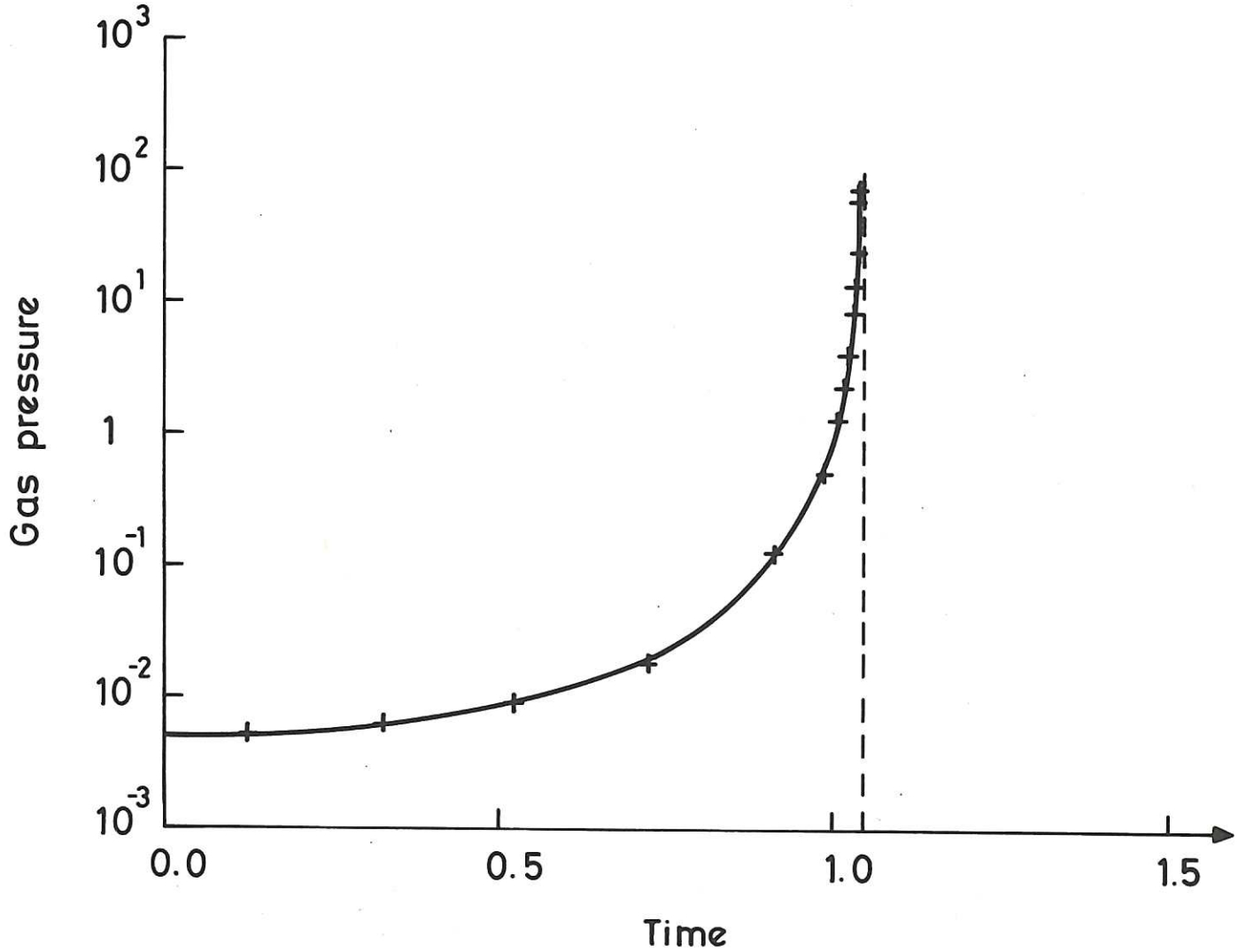

Fig.7 Variation of gas pressure within the cavity of Fig.6 vs time. The extremely high pressures reached near the time of collapse do not significantly retard the jet, which reaches a final maximum velocity of 16.5 units.